Surface Wave Tomography of China from Ambient Seismic Noise Correlation

Sihua Zheng[1,2], Xinlei Sun[2], Xiaodong Song[2]*, Yingjie Yang[3], and Michael H. Ritzwoller[3]

1. Institute of Earthquake Science, China Earthquake Administration, Beijing, China
2. Department of Geology, University of Illinois, Urbana, IL, USA
3. Department of Physics, University of Colorado at Boulder, CO, USA

* Correspondence: xsong@uiuc.edu

To be submitted to GRL

Abstract. We perform ambient noise tomography of China using the data from the China National Seismic Network and surrounding global and regional stations. For most of the station pairs, we retrieve good Rayleigh waveforms from ambient noise correlations using 18-months of continuous data at all distance ranges across the entire region (over 5000 km) and for periods from 70 s down to about 8 s. We obtain Rayleigh wave group velocity dispersion measurements using a frequency-time analysis method and invert for Rayleigh wave group velocity maps for periods from 8 s to 60 s. The tomographic maps display significant features that correlate with surface geology. Two major features stand out in particular. First, the major basins with thick sedimentary deposits correlate well

with slow group velocities at shorter periods (10 to 20 s). The major basins, including Tarim, Junggar, Qadaim, Sichuan, Bohai-Wan, and Songliao, are all well delineated by slow group velocities. Second, variations in crustal thickness correlate with group velocities for periods around 30 s. The major trend of crustal thickening from the east to west is well represented by group velocity decreases from east to west.

1. INTRODUCTION

Recent theoretical and laboratory studies have shown that the Green functions of a structure can be obtained from the cross-correlation of diffuse wavefields (e.g., Lobkis and Weaver, 2001; see also review Campillo, 2006). The basic idea is that linear waves preserve, regardless of scattering, a residual coherence that can be stacked and amplified to extract coherent information between receivers (e.g., Weaver, 2005). The idea has now found rapid applications in seismology. In particular, surface waves have been found to be most easily retrievable from the cross-correlations of seismic coda (Campillo and Paul, 2003; Paul et al., 2005) or ambient noise (Shapiro and Campillo, 2004; Shapiro et al., 2005; Sabra et al., 2005a, 2005b) between two stations. Both Rayleigh waves and Love waves can be retrieved. The new type of data have rapidly been used for tomographic mapping at regional or local scales (e.g., Shapiro et al., 2005; Sabra et al., 2005b; Kang and Shin, 2006; Villaseñor et al., 2007; Liang and Langston, 2007) and on continental scales (e.g., Yang et al., 2007; Bensen et al., 2008). These studies have focused on Rayleigh wave group velocity tomography from ambient noise. However, the

method has been demonstrated to be applicable to Love waves (Lin et al., 2008) and phase velocity measurements (Yao et al., 2006; Lin et al., 2008).

Ambient noise tomography (ANT) overcomes several important limitations of conventional methods based on earthquakes; i.e., uneven distribution of earthquake sources, uncertainty in earthquake location, and attenuation of short-period surface waves. Thus, the method is particularly useful for surface-wave path calibration and for tomographic mapping in aseismic regions especially at short periods (below 30 s). Here we obtain inter-station dispersion measurements and perform ANT of China using stations from the China National Seismic Network (CNSN) and (Figure 1). The CNSN is the national backbone network, established around 2000, with a relatively uniform distribution across the Chinese continent. To increase data coverage, we also include a few stations in the surrounding regions. We focus on Rayleigh wave group velocities in this study.

2. DATA AND METHOD

We use 18 months of continuous data from 47 CNSN stations and 12 other stations. All stations are broadband. The bandwidths of the CNSN stations are from 20 Hz to at least 120 s. We use the data processing and imaging techniques described in detail by Bensen et al. (2007). Below is a brief outline of our data procedure. First, we obtain the empirical Green function (EGF) from ambient noise cross-correlation. Continuous data are pre-

processed before correlation and stacking, which includes clock synchronization, removal of instrument response, time-domain filtering, temporal normalization and spectral whitening. The purpose is to reduce the influence of earthquake signals and instrument irregularities and to enhance the strength and bandwidth of the ambient noise correlations. Second, if the signal-to-noise ratio (SNR) is sufficiently large, Rayleigh wave group speeds are measured using a frequency-time analysis (Ritzwoller and Levshin, 1998). Finally, the inter-station dispersion measurements are used to invert for the Rayleigh wave group velocity maps, in exactly the same way as earthquake-based measurements.

3. RESULTS

For most of the station pairs, we are able to retrieve good Rayleigh wave signals from the ambient noise correlations. Figure 2 shows typical examples of EGFs and group velocity measurements of Rayleigh waves retrieved from ambient noise correlations. The cross-correlations show strong arrivals at different settings (near the coast or well into the continental interior) and at both relatively low frequencies (20-50 s) and high frequencies (5-20 s). The EGFs can be retrieved over the entire region (at distances of over 5000 km) (Figure 2a).

We measured group velocity dispersion curves (Figure 2c) for station pairs with Rayleigh wave SNR>10. The SNR is defined as the ratio of the peak amplitude of the Rayleigh wave to the root-mean-square value of the background. The measurement is very stable. Clear dispersion can be commonly observed directly from the EGFs (Figure 2b). We

found that the group velocity measurements can extend to periods of 10 s or shorter even for station pairs that are separated over thousands of kilometers. The group velocities of the HTA-BRVK path (Figure 2b,c), which samples the Tarim Basin, agree with a global 3D earthquake-based model (Shapiro and Ritzwoller, 2002) at longer periods but differ significantly at short periods (below 30 s). The slow group velocities at short periods are caused by the thick sediments of the Tarim Basin (see discussion below).

We have obtained dispersion measurements with SNR>10 for periods 8 s to 70 s (auxiliary material Figure S1a). The best observed frequency band is 10 to 30 s with over 1000 measurements at each period or a retrieval rate of 50 to 80% of all the possible pairs. The ray paths cover almost the entire Chinese continent (auxiliary material Figure S1b). However, the coverage is much better in the eastern half of the country, because of the denser station distribution there than in the western part.

The ray coverage of our dispersion measurements is sufficient for us to invert for Rayleigh wave group velocity maps at periods from 8 s to 60 s (Figure 3). The results show remarkable features that correlate with large-scale geological structures of China. Major basins are well delineated with low velocities at short periods (8 to 20 s), including Bohai-Wan Basin (North China Basin), Sichuan Basin, Qaidam Basin, and Tarim Basin. The stable Yangtz Craton also shows up well with high velocities. At longer periods (25-50 s), the group velocity maps display striking bimodal distribution with high velocity in the east and low velocity in the west, which corresponds very well with the thinner crust in the east and much thicker crust in the west (e.g. Liang et al., 2004). The NNE-SSW

112 trending boundary between fast and slow velocities (around longitude 108^{o}E) coincides
113 with the sharp topographic change and with the well-known Gravity Lineation.
114
115 A side-by-side comparison between a short period group velocity map and sediment
116 thickness or between an intermediate period map and crustal thickness is presented in
117 Figure S2 of the auxiliary material. The correlations are quite striking if we compare the
118 group velocities along a certain profile of interest (Figure 4). The selected profile along
119 latitude of about 39^{o}N passes through three major basins: Tarim, Ordos, and Bohai-Wan
120 (Figure 1). The thick sediments in these basins (Laske and Masters, 1997) correlate well
121 with slow velocities at periods from 10 to 20 s (Figure 4a). The general trend of
122 decreasing crustal thickness from west to east is well represented by increasing group
123 velocities around 30 s (Figure 4b). However, the group velocity map displays more
124 structure than the smooth crustal thickness curve from the global reference model
125 (CRUST 2.0) (http://mahi.ucsd.edu/Gabi/rem.html), suggesting a more complex Moho.
126 At period 50 s, the trend is no longer observable as the surface waves sample deeper into
127 the mantle.
128
129

130 ## 4. CONCLUSION AND DISCUSSION

131 Using correlations of 18 months of continuous data from CNSN and global seismic
132 stations, we retrieve Rayleigh wave empirical Green functions (EGFs) over a broad
133 frequency band across China and surroundings. Group velocity dispersion measurements

are obtained for periods of 8 to 70 s. The best observed frequency band is 10 to 30 s with a retrieval rate of 50 to 80% of the station-pairs. We have constructed Rayleigh wave group velocity maps of China from 8 to 60 s. The tomographic maps show remarkable correlations with the major tectonic features of China, in particular, the major sedimentary basins and crustal thickness.

Comparison of the tomographic maps with the geological features discussed above provides an important validation of the ambient noise tomography (ANT) methodology; i.e., the method provides models of group wave speeds that are consistent with well-known geological features and other geophysical observations. Furthermore, the complete repeatability of the ANT method makes it possible to validate directly the methodology and to evaluate the uncertainties of the dispersion measurements. Several methods have been proposed in this regard. (1) Direct verification: Comparing the EGF with the surface wave generated by an earthquake along the same path (e.g., Shapiro et al., 2005; Bensen et al., 2007). (2) Comparing the EGF obtained from ambient noise and that from seismic coda (Yao et al., 2006). (3) Temporal stability: Comparing the EGFs from the data observed at different time periods (e.g., different months) (Shapiro et al., 2005; Yao et al., 2006; Bensen et al., 2007). Furthermore, because the principal ambient noise sources are believed to come from the oceans (e.g., Yang et al., 2008), which are seasonal, the consistency of the correlations from different seasons gives a measure of the stability and error of the EGFs (Bensen et al., 2007). (4) Spatial consistency: Comparing the EGFs for station-pairs along similar paths (Bensen et al., 2007). The EGFs between a far-away station to two or more stations that are close to one another should be similar as

the paths sample similar structure. We have examined temporal and spatial consistency of our dispersion measurements and found that they are very consistent whenever the SNRs of the EGFs are high. Some examples are shown in Figure S3 of the auxiliary material.

Acknowledgments. The CNSC waveform data were provided by China Earthquake Network Center and other station data were obtained from IRIS DMC. The figures were made using GMT software (Wessel and Smith, 1998).

REFERENCES

Benson, G., M. Ritzwoller, M. Barmin et al., Processing seismic ambient noise data to obtain reliable broad-band surface wave dispersion measurements, *Geophys. J. Int.*, 169(3), 1239-1260, 2007.

Bensen, G.D., M.H. Ritzwoller, and N.M. Shapiro, Broad-band ambient noise surface wave tomography across the United Stated, *J. Geophys. Res.*, in press, 2008.

Campillo, M. Phase and correlation in random seismic fields and the reconstruction of the Green function, *Pure Appl. Geophys.*, 163, 475-502, 2006.

Campillo M. and A. Paul, Long-range correlations in the diffuse seismic coda, *Science*, 299, 547-549, 2003.

Kang, T.S. and J.S. Shin, Surface-wave tomography from ambient noise of accelerograph networks in southern Korea, *Geophys. Res. Lett.*, 33 (17): Art. No. L 17303, 2006.

Laske, G., and G. Masters, A global digital map of sediment thickness, EOS Trans. AGU, 78, F483, 1997.

178 Liang, C.T., and C.A. Langston, Ambient seismic noise tomography and structure of eastern
179 North America, J. Geophys. Res., in press, 2007.
180 Liang, C.T., X.D. Song, J.L. Huang, Tomographic inversion of Pn travel times in China, *J.*
181 *Geophys. Res.*, 109, B11304, doi: 10.1029/2003JB002789, 2004.
182 Lin, F., M.P. Moschetti, and M.H. Ritzwoller, Surface wave tomography of the western
183 United States from ambient seismic noise: Rayleigh and Love wave phase velocity
184 maps, *Geophys. J. Int.*, in press, 2008.
185 Lobkis, O.I., and R.L. Weaver, On the emergence of the Greens function in the correlations
186 of a diffuse field, *J. Acoust. Soc. Am.*, 110, 3011-3017, 2001.
187 Paul, A., M Campillo, L. Margerin and E. Larose (2005) Empirical synthesis of time-
188 asymmetrical Greens functions from the correlation of coda waves, *J. Geophys. Res.*,
189 110, B08201, doi: 10.1029/2004JB0035231.
190 Ritzwoller, M.H. and A.L. Levshin, Eurasian surface wave tomography: Group velocities, *J.*
191 *Geophys. Res.*, 103, 4839-4878, 1998.
192 Sabra, K.G., P. Gerstoft, P. Roux, W.A. Kuperman, and M.C. Fehler, Extracting time domain
193 Green's function estimates from ambient seismic noise, *Geophys. Res. Lett.* 32, doi:
194 10.1029/2004GL021862, 2005a.
195 Sabra, K.G., P. Gerstoft, P. Roux, W.A. Kuperman, and M.C. Fehler, Surface wave
196 tomography from microseisms in Southern California, *Geophys. Res. Lett.*, 2005b.
197 Shapiro, N.M. and M.H. Ritzwoller, Monte-Carlo inversion for a global shear velocity model
198 of the crust and upper mantle, *Geophys. J. Int.*, 151, 88-105, 2002.

199 Shapiro, N.M. and M. Campillo, Emergence of broadband Rayleigh waves from correlations
200 of the ambient seismic noise, *Geophys. Res. Lett.*, 31, L07614, doi:
201 10.1029/2004GL019491, 2004.
202 Shapiro, N.M. M. Campillo, L. Stehly, and M.H. Ritzwoller, High resolution surface wave
203 tomography from ambient seismic noise, *Science*, 307(5715), 1615-1618, 2005.
204 Weaver, R.L., Information from Seismic Noise, *Science*, 307, 1568-1569, 2005.
205 Villaseñor, A., Y. Yang, M.H. Ritzwoller, and J. Gallart, Ambient noise surface wave
206 tomography of the Iberian Peninsula: Implications for shallow seismic structure,
207 *Geophys. Res. Lett.*, 34, L11304, doi:10.1029/2007GL030164, 2007.
208 Yang, Y.J., M.H. Ritzwoller, A.L. Levshin, and N.M. Shapiro, Ambient noise Rayleigh wave
209 tomography across Europe, *Geophys. J. Int.* 168, 259-274 doi: 10.1111/j.1365-
210 246X.2006.03203.x, 2007.
211 Yang, Y. and M.H. Ritzwoller, The characteristics of ambient seismic noise as a source for
212 surface wave tomography, *Geochem., Geophys., Geosys.*, in press, 2008.
213 Yao, H.J., R.D. van der Hilst, and M.V. de Hoop, Surface-wave array tomography in SE
214 Tibet from ambient noise and two-station analysis - I. phase velocity maps, *Geophys. J.*
215 *Int.*, 166(2) 732-744, 2006.
216
217
218
219

FIGURE CAPTIONS

Figure 1. Distribution of seismic stations used in this study, including China National Seismic Network (CNSN) stations (open triangles) and stations in the surrounding regions (solid triangles). Plotted also are major tectonic boundaries (from Liang et al., 2004) and major basins. The basins that are labeled include: Tarim (TRM), Junggar (JG), Qaidam (QD), Sichuan (SC), Ordos (OD), Bohai Wan (BHW), and Songliao (SL) Basins. The thick dashed-line across northern China from the Tarim Basin to Korea indicates the selected great-circle path for Figure 4.

Figure 2. Example of Rayleigh wave EGFs and dispersion measurements obtained from ambient noise correlations. (a) Symmetric component of the correlations between station QIZ (in Hainan Province, China) and other stations. The traces are band-pass filtered at relatively short periods (10-30 s). (B) EGFs filtered in different frequency bands. Long-period surface waves are clearly faster than short-period ones. The path is between HTA (bordering Tarim in the south) and BRVK (Borovoye, Kazakhstan). (C) Frequency-time analysis (Ritzwoller and Levshin, 1998) used to retrieve Rayleigh wave group velocity dispersion curve (white) for the HTA-BRVK path. The black dashed curve is the prediction from the 3D global shear velocity model of Shapiro and Ritzwoller (2002), which is used for phase-matched filtering in the data analysis and for comparison with measurements.

Figure 3. Maps of Rayleigh wave group velocities at periods of 8, 12, 20, 30, 45, and 60 s. Note the color scale for each period is selected so that the scale represents the range of the values with the average value in the middle of the color bar (between yellow and green). The ranges of the values for different periods are different.

Figure 4. Rayleigh wave group velocities are compared with sediment thickness (**a**) and crustal thickness (**b**) along a selected path. The selected path is along the great-circle path between (38^{o}N, 80^{o}E) and (38^{o}N, 125^{o}E), passing through three major basins (Tarim, Ordos, and Bohai Wan) (Figure 1). Plotted at the top are velocities for shorter periods (**a**) and for longer periods (**b**), respectively. Plotted at the bottom are sediment thickness (**a**) and crustal thickness (**b**), respectively. In the middle are surface elevations.

Fig. 1

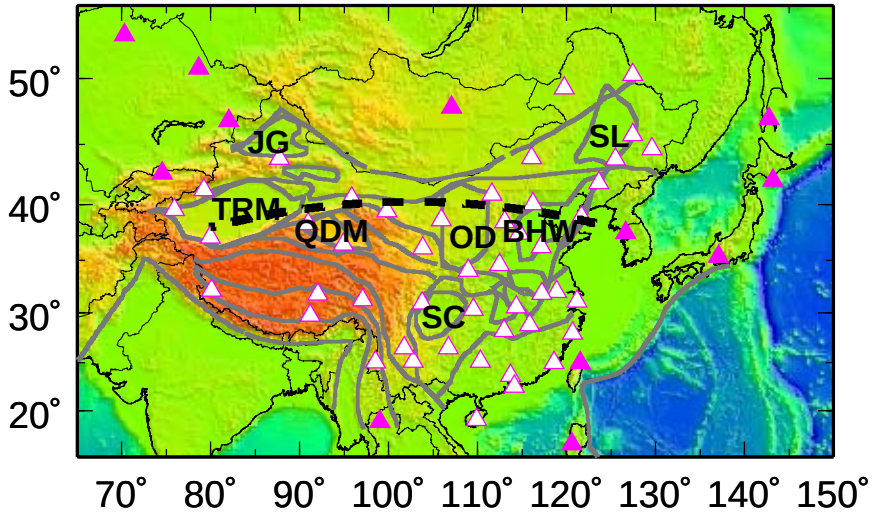

Fig. 2

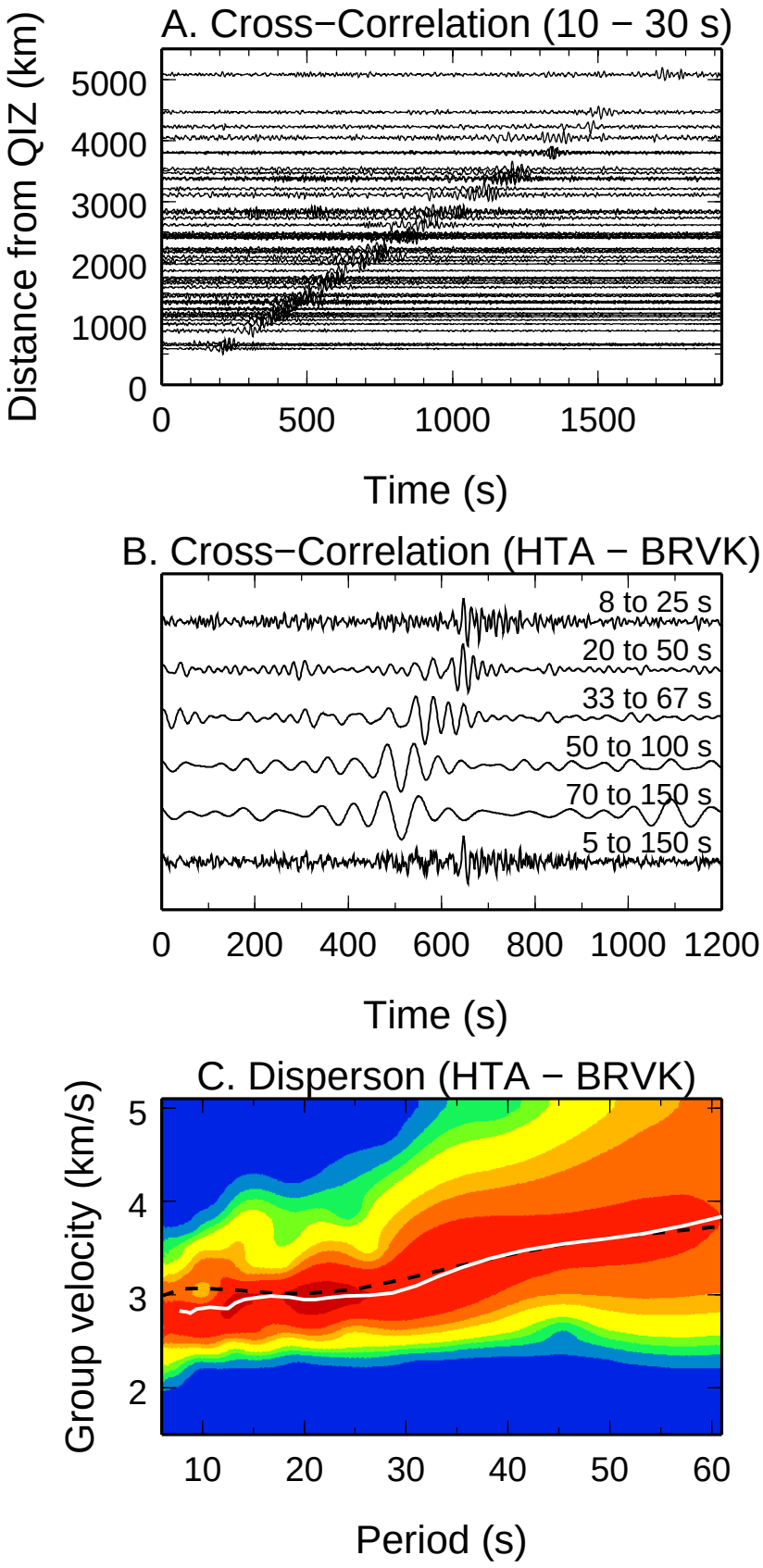
A. Cross−Correlation (10 − 30 s)
Distance from QIZ (km)
5000
4000
3000
2000
1000
0
0
500
1000
1500
Time (s)
B. Cross−Correlation (HTA − BRVK)
8 to 25 s
20 to 50 s
33 to 67 s
50 to 100 s
70 to 150 s
5 to 150 s
0
200
400
600
800
1000
1200
Time (s)
C. Disperson (HTA − BRVK)
Group velocity (km/s)
5
4
3
2
10
20
30
40
50
60
Period (s)

Fig. 3

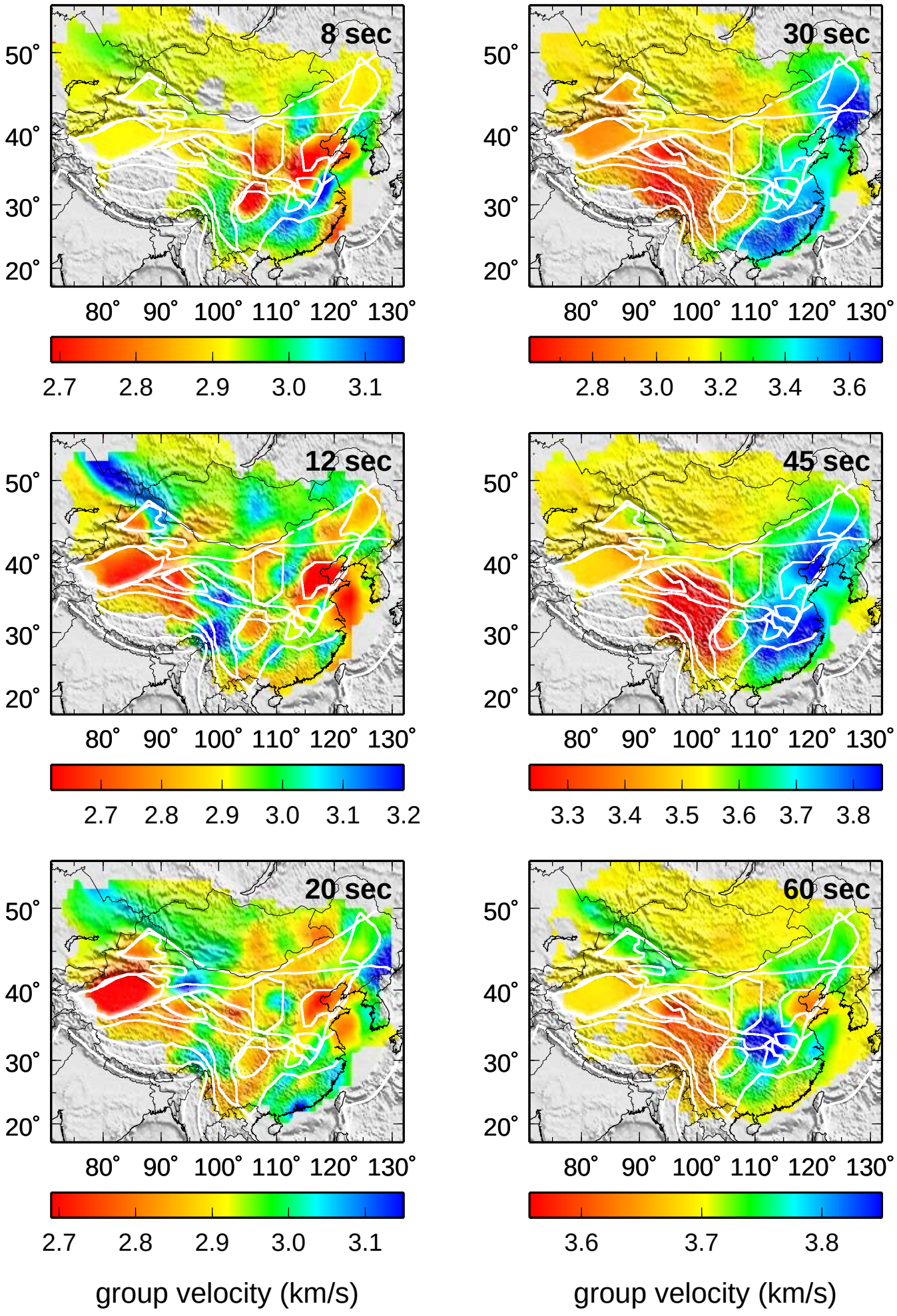
8 sec
30 sec
12 sec
45 sec
20 sec
60 sec
50°
40°
30°
20°
80° 90° 100° 110° 120° 130°
2.7 2.8 2.9 3.0 3.1
2.8 3.0 3.2 3.4 3.6
2.7 2.8 2.9 3.0 3.1 3.2
3.3 3.4 3.5 3.6 3.7 3.8
2.7 2.8 2.9 3.0 3.1
3.6 3.7 3.8
group velocity (km/s)
group velocity (km/s)

Fig. 4

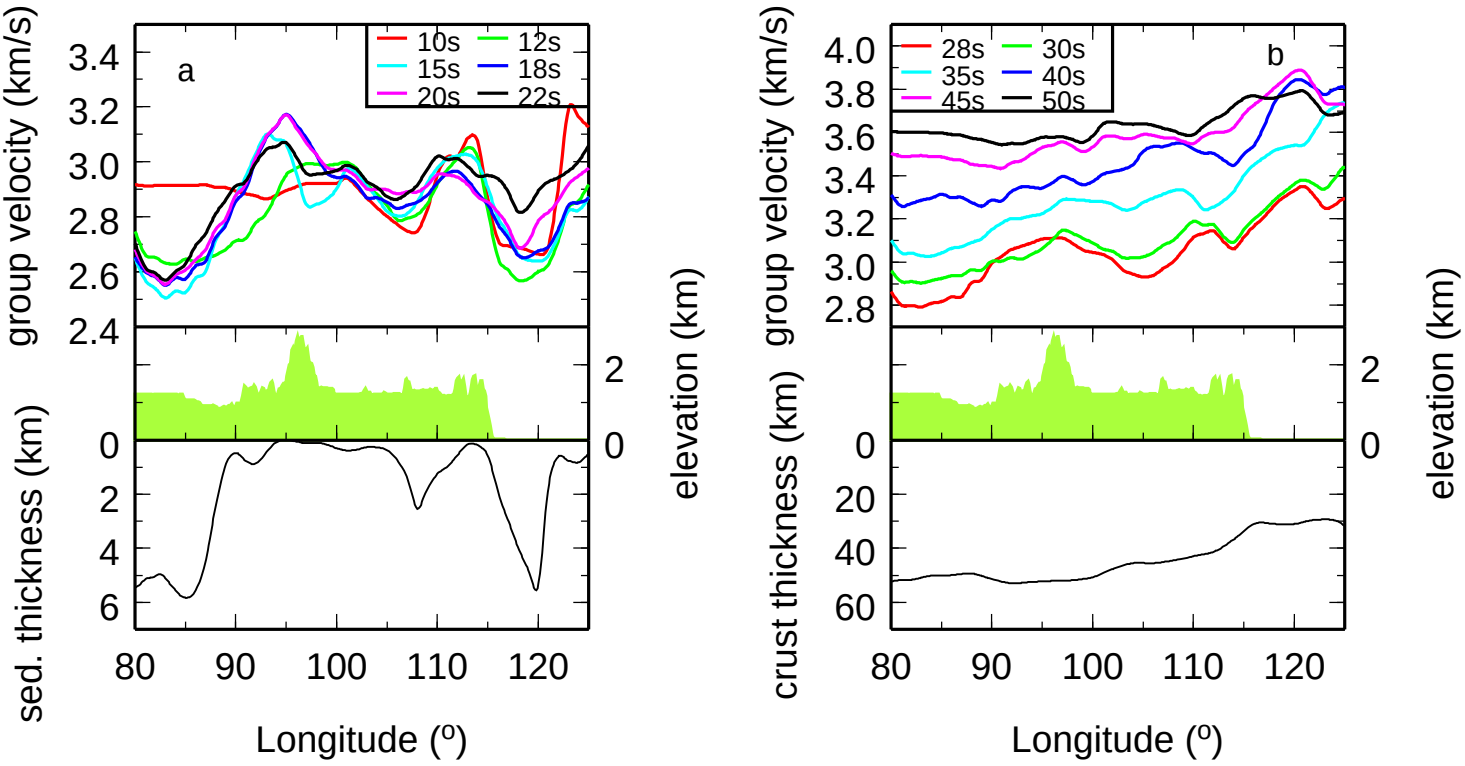
a
10s
12s
15s
18s
20s
22s
group velocity (km/s)
3.4
3.2
3.0
2.8
2.6
2.4
2
0
sed. thickness (km)
0
2
4
6
elevation (km)
80
90
100
110
120
Longitude (º)
b
28s
30s
35s
40s
45s
50s
group velocity (km/s)
4.0
3.8
3.6
3.4
3.2
3.0
2.8
2
0
crust thickness (km)
0
20
40
60
elevation (km)
80
90
100
110
120
Longitude (º)